Optical and dielectric studies of Zn doped cerium nanocomposite

T.R.Sherly[1]*, R.Raveendran[2]
[1]Post Graduate Department of Physics, Sanathana Dharma College, Alappuzha, Kerala, - 688003, (INDIA)
[2]Nanoscience Research Laboratory, Sree Narayana College, Kollam, Kerala, – 691001, (INDIA)
E-mail : trsherly@gmail.com

ABSTRACT

Cerium phosphate was synthesized by co-precipitation method – the base salt. This base salt was doped with zinc having different molarities. Their structure and morphology were characterized by X- ray diffraction (XRD), Fourier transform infra red spectroscopy (FTIR), scanning electron microscopy (SEM) and transmission electron microscopy (TEM). Optical properties were analyzed by UV – Visible absorption and diffuse reflectance spectra, Raman spectra and Photoluminescence spectra. The observed photoluminescence of the sample is attributed to various defects resulting from crystallization and also due to the amount of Ce^{3+} in mixed oxide system. Violet, Blue, Green emissions were observed which make our samples useful in photonic devices. Ion exchange studies were carried out on protonated base sample. Chemical composition was obtained with energy dispersive X- ray spectroscopy (EDS). Dielectric constant and loss tangent were determined. Thermal stability analyzed with TGA/DTA.
© 2014 Trade Science Inc. - INDIA

KEYWORDS

Cation;
Dielectric material;
Photonic device;
Cerium phosphate;
Photoluminescence;
Nanomaterials.

INTRODUCTION

Now a day's inorganic ion exchange materials are gaining much importance owing to their ability to remove pollutants, especially environmental ones. Tetravalent metal acid (TMA) salts are novel materials amongst inorganic ion exchangers and can be synthesized in both amorphous and crystalline form[1-6]. Cerium compounds have received special attention for various applications owing to their redox properties ($Ce^{4+} \leftrightarrow Ce^{3+}$), catalytic activity, elevated oxygen transport, oxygen storage capacity (OSC) and more over their thermal stability. Although, numerous ion exchangers in the bulk form have been reported earlier, the ion exchanging property, dielectric study, luminous property and UV absorbing property of cerium based inorganic ion exchange materials in the nano form have relatively been untouched. Certain other ion exchangers were prepared by our group[7-9], now we could improve the crystalline nature of the product. In the present study, cerium phosphate, in nano form was prepared by co-precipitation method. It was doped with Zn of different molarities.

EXPERIMENTAL

Material and methods

In the present endeavour, Cerium phosphate has been synthesized by co- precipitation method. Aque-

ous solution of Ammonium ceric sulphate and disodium hydrogen phosphate in appropriate molar ratios were used as starting materials. Ammonium ceric sulphate and disodium hydrogen phosphate were obtained from Merck or BDH and used without further purification. All reagents used were of GR or AR grade. Ethylene diamine tetra acetic acid (EDTA) was used as a capping agent to stabilize the particle against agglomeration. The precipitated sample was washed several times with distilled water and then with ethanol. The sample, cerium phosphate is allowed to dry naturally, and this is base sample P. The base sample P was doped with zinc of different molarities (0.01, 0.02, 0.03, 0.04 M) and the sample codes were F1, F2, F3, and F4 respectively. The crystal structure, phase purity, morphology and chemical composition of the prepared samples were

characterized by XRD, SEM, TEM, FTIR and EDS studies. The cation exchange property of sample P has been explored by column method. In addition, UV absorbance – diffuse reflectance, photoluminescence, Raman studies and dielectric studies were also investigated. Thermal stability was analysed with TGA/DTA.

RESULTS AND DISCUSSIONS

X – ray diffraction analysis

X- ray diffraction (XRD) pattern of the samples were recorded in the 2θ range from 10° to 60° at an incidence angle of 1° with Bruker AXS D8 Advance diffractometer. XRD profiles of the as prepared and doped samples are shown in Figure 1. All the peaks in sample P were indexed to anorthic phase of $CePO_4$. These were compa-

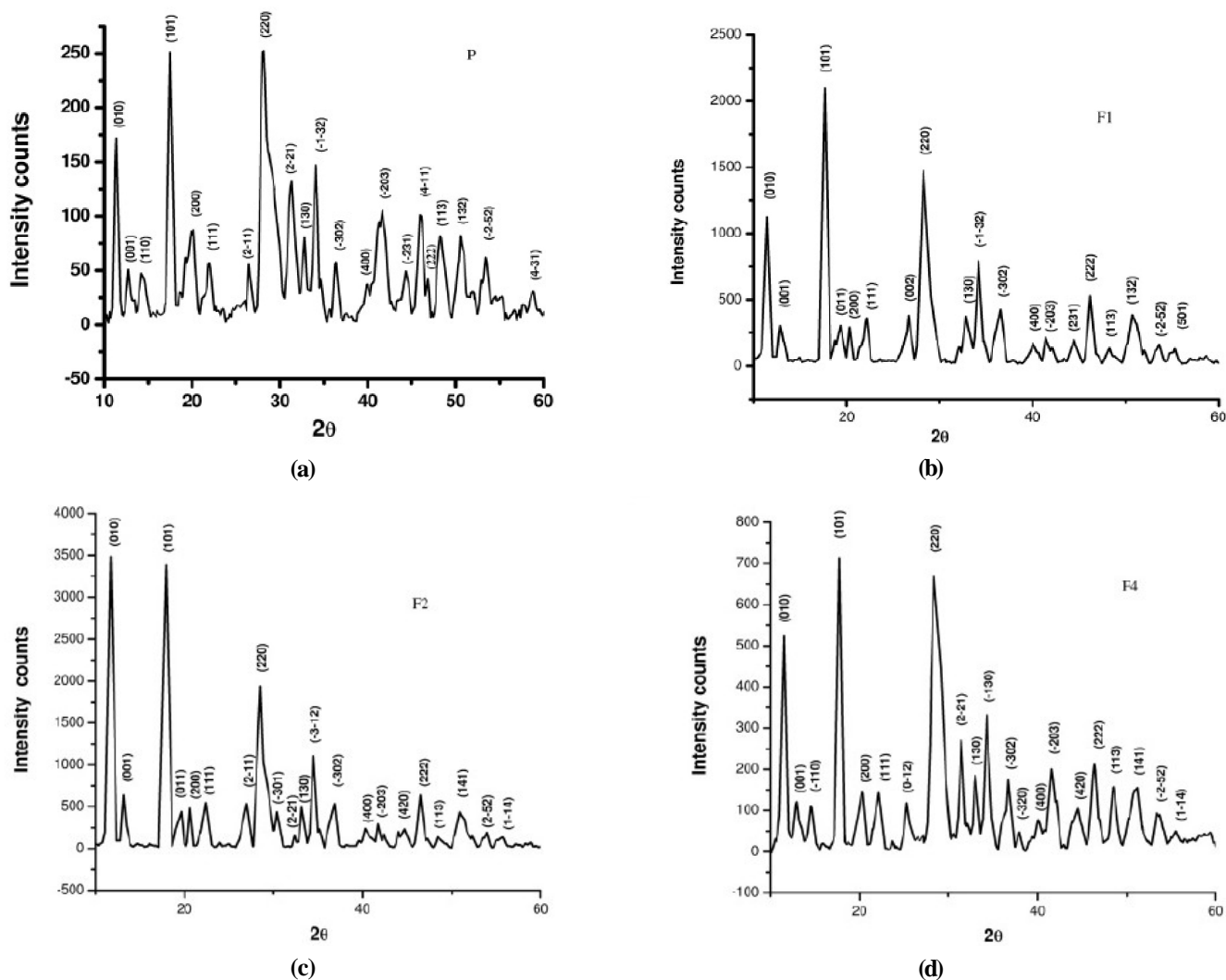**(a)**

(b)

(c)

(d)

Figure 1 : X- ray diffraction pattern of samples 1(a) P, 1(b) F1, 1(c) F2 and 1(d) F4. Anorthic structure remains stable w.r.to doping. No impurity phases were observed

Full Paper

rable with the values from JCPDS 77-1507. Zinc doped samples also exhibit anorthic phase with no other impurity phases. Some amount of peak shifting was observed in doped samples. XRD profiles indicate that the prepared samples are crystalline in nature and broadening in the peaks indicates that the crystallites are smaller in size. From XRD profile micro structural parameters such as crystallite size, dislocation density, micro strain and elastic strain were calculated.

SEM analysis & chemical composition (EDS)

The surface morphology of the sample was obtained by scanning electron microscope (SEM) on a JEOL Model JSM - 6390LV scanning electron microscope and Elemental composition (EDS) on a JEOL Model JED – 2300 energy dispersive spectrometer. SEM image provides information on the morphology of the prepared sample. It is inferred from the SEM micrograph, that particles are rod shaped and evenly distributed. This was confirmed with TEM image Figure 3(a). Chemical composition and product purity of the prepared sample was confirmed by EDS, Figure 2. EDS is an analytical technique used for the elemental analysis or chemical characterization of a sample. Qualitative analysis involves the identification of the lines in the spectrum. Quantitative analysis (determination of the concentration of the elements present) involves measuring the line intensities for each element in the sample. In addition to cerium and phosphorous peaks, a peak due to oxygen was observed in our sample, which can be assigned due to the oxygen storage capacity of the prepared sample. Since Cerium compounds can become non – stoichiometric in oxygen content, it can give up oxygen without decomposing or it can release or take in oxygen. During rich conditions, Ce^{4+} is reduced to Ce^{3+} and releases Oxygen. During lean conditions, it takes up O and the reverse reaction occurs. It is reported that Cerium compounds were promising candidates for catalytic application owing to this property[10,11]. EDS, [Figure 2] shows the presence of Cerium at 0.8eV (M_α line), 4.839 eV (L_α line), 5.199 eV, 5.599 eV (L_β line). Phosphorous at 2.013 eV (K_α line) and Oxygen at 0.525 eV (K_α line) with no impurity peaks present.

This confirms purity of the prepared sample. From EDS analysis percentage of each elements present in the sample were calculated and is presented in TABLE 1.
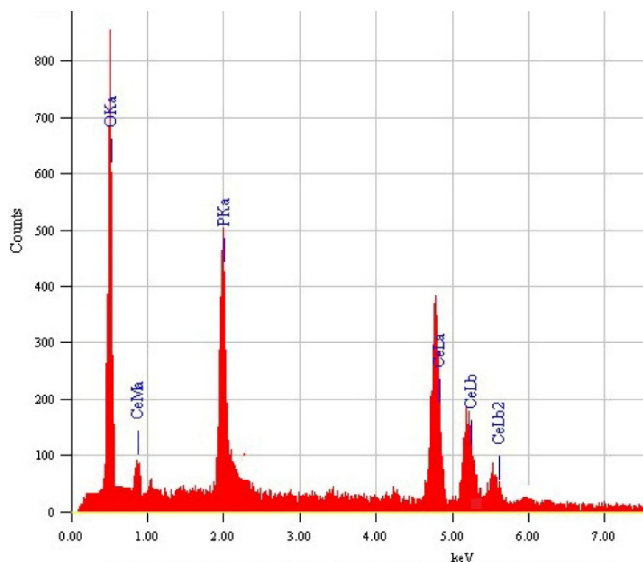

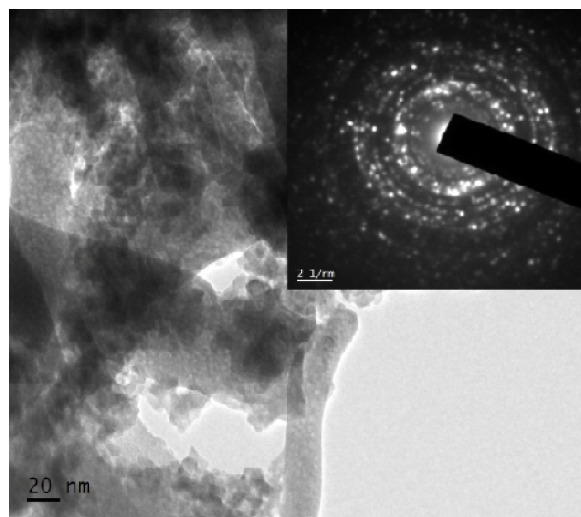Fig. 2 EDS of sample P. No impurity peaks were present

Fig 3(a) TEM Image of CePO₄ nanorods ,(Insets)SAED pattern

Fig 3(b) HRTEM image shows lattice fringes

Full Paper

TEM analysis

HRTEM image is obtained with JEOL JEM 2100. Figure 3(a) is the TEM image and SAED pattern of cerium phosphate nano rods.

TABLE 1 : Chemical composition of sample P from EDS analysis

Element / Shell	keV	Mass %	Atom %
Oxygen K	0.525	51.76	78.31
Phosphorous K	2.013	21.94	17.15
	0.800		
Cerium L	4.839	26.3	4.54
	5.199		

Fig 3(b) is the HRTEM image displays lattice fringes, indicating highly crystalline nature of the material. From the figure it is clear that slight agglomeration of particles, which can be due to the fact that materials synthesized in water medium becomes agglomerated due to high capillary forces and hydrogen bonding of water.

water. The total weight loss corresponds to two molecule of water (7.793 %), present as water of crystallization, which is in close agreement with the theoretical value calculated (7.515 %). From DTA curve peak temperature is $100°$ C.

Second stage of decomposition is from $158°$ C to $211.5°$ C. The mass loss in this stage is 13.617 %, which corresponds to the removal of two molecule of oxygen out of the whole sample. Theoretically it is about 13.36 %. Peak temperature is $188.97°$C.

Third stage of decomposition stars from $212°$ C to $857°$ C. Peak temperature in this stage is $786.84°$ C. Total mass loss during this stage is found to be 39.847 % (13.617 + 26.23). These two stages are attributed to the decomposition of the phosphate molecule (Theoretically it is 39.66 %), and its elimination. On further heating, there is no significant loss is observed which indicates the stability of the metal oxide system.
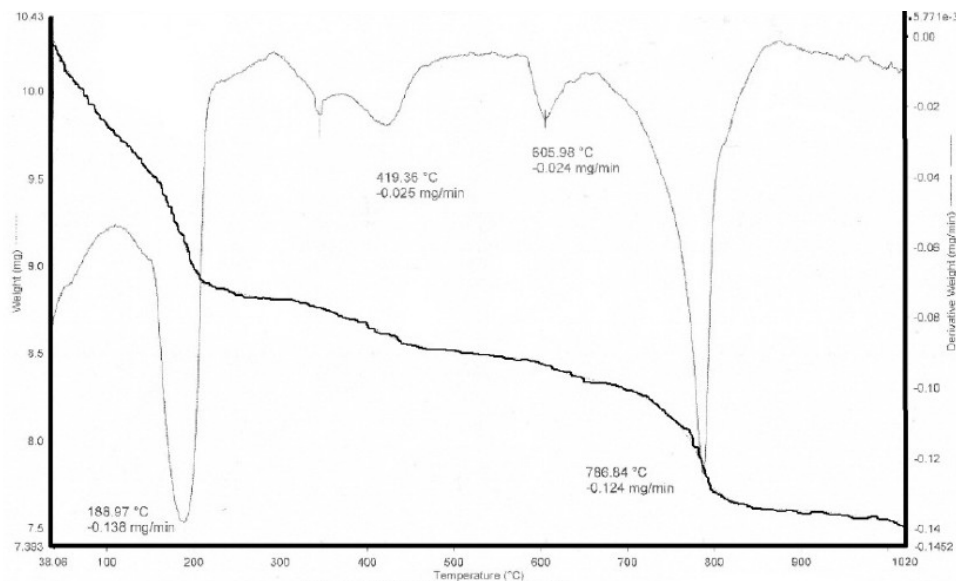

Fig 4 TGA/DTA curve of sample P

TGA/DTA analysis

Thermo gravimetric analysis was done on Perkin Elmer, Diamond TG/DTA. Sample was heated from $40°$C to $1020°$C, at a heating rate of $10°$C/min in Nitrogen atmosphere. The TGA/DTA curves for sample P is shown in Figure 4. The first stage of decomposition starts from $41°$C and ends at $100°$C. The mass loss is 4.822 % corresponds to the loss of a molecule of water (Theoretically it is 3.8 %). The next stage is from $100°$C to $157.69°$C. The mass loss is 7.793 % which corresponds to the removal of another molecule of

UV – Vis and DRS studies

Optical reflectance and absorbance data of the samples were measured in the range of 200 – 2000 nm using a Varian, Cary 5000 spectrophotometer having a resolution of 0.05 nm. To analyze the electronic properties of the prepared sample Kubelka – Monk function F(R) was[12,13] used, where R is the diffuse reflectance of a given wavelength. Figure 5 shows UV – Vis absorption spectra of cerium phosphate and doped cerium phosphate nanoparticles.

Absorption spectra show a peak at 275 nm which

Full Paper
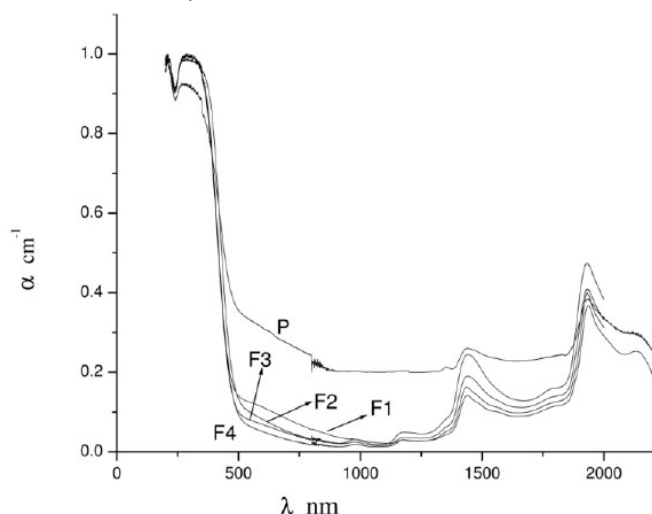
Figure 5 : Absorption spectra of samples P, F1, F2, F3 and F4. Blue shift is observed in doped samples

is the characteristic absorption[11,14,15] peak of Ce^{3+}. This was in close agreement with the theoretical value (203 – 276 nm) of Ce^{3+}. This can be explained as due to the f – d transition from 4f^1 ground state to the 5d^1 state of Ce^{3+}. Absorption spectra show that samples were almost transparent in the visible region and absorb ultraviolet radiation strongly and slight absorption in the IR region. On doping, transparency in the visible region increases, UV absorbance increases considerably, and blue shift is predominantly observed in the doped samples. As a result band gap shifts to higher value. Important requirements for the UV shielding nano material are that it should absorb UV radiation strongly and should possess a cut off wavelength nearly between 350- 400 nm. This means energy band gap[16] should approximately in between 3 – 4 eV. Moreover material is to be transparent in the visible region. These requirements agree well with our results. So we suggest this material as a good candidate for sunscreens.

The relation between the absorption coefficient (α) and the incident photon energy hυ[17] is given by, $(\alpha h\upsilon)^2 = k (h\upsilon – E_g)$, where k is proportionality constant, α is the optical absorption coefficient and E_g is the band gap. The band gap is determined by extrapolation of the linear portion of $(\alpha h\upsilon)^2$ versus (hυ) plot as shown in Figure 6. Two distinct band gap values were obtained in doped samples, one is the actual band gap and the lower value corresponds to transition from defect level. From Figure 6, it is clear that in doped samples, additional levels are created in between valence band and

conduction band, schematically this was depicted in Figure 6(d). This may be due to the fact that on doping with zinc, defects levels and oxygen vacancies are created and which modify the density of states in the system, results in modified band gap. This can also be confirmed with PL studies. The energy band gaps of the samples are 2.8, 3.6, 3.73, 3.87 and 4 eV.

Photoluminescence analysis

Photoluminescence measurements were done on a Perker Elmer LS 45 Fluorescent Spectrometer. Figure 7 shows the photoluminescence (PL) spectra of undoped and doped samples.

On excitation with 290 nm, the undoped sample gives a broad PL peak in the visible region and for doped samples peaks around 456 – 480 nm (blue), 528 nm (green) which are characteristic of the Ce^{3+} state were observed. In addition to these bands, 330 – 375 nm (near - band- edge emission), 420 nm (violet) were also observed. Green emission band arise from the recombination of photo generated hole with a singly ionized defect such as oxygen vacancy[18]. In doped samples, photoluminescence increases and luminescence property changes from visible to ultraviolet region. This implies that on doping more defect levels are introduced in the samples and the concentration of the Ce^{3+} ions are increased. This is also observed in UV studies. There are lots of oxygen vacancies and defect energy levels exist between Ce '4f' and O '2p' level which is responsible for the broad PL peak. Electrons were trapped in defects levels, which results in the formation of F center and these electrons were transmitted from defect level to O 2p level and forms peak around 330 – 375 nm, which is the near- band- edge (NBE) emission. Near – band – edge emission can also be due to the recombination of free or bound excitons[18]. Violet and Blue emissions[15] are reported earlier in the case of Cerium phosphate nanofiber and cerium oxide thin film[19,20]. In Cerium ion, 4f electrons are well shielded from external charge by 5s^2 and 5p^6 shells. Optical properties of the rare earth ions are due to transition of the shielded inner 4f electrons[21]. Such shielding leads to discrete and well defined energy levels and resultant transition leads to multiple peaks. Blue emission can be attributed to the de – excitation of Ce^{3+} ions from $^5D_{3/2}$ excited state to the split ground state $^4F_{5/2}$ and $^4F_{7/2}$.
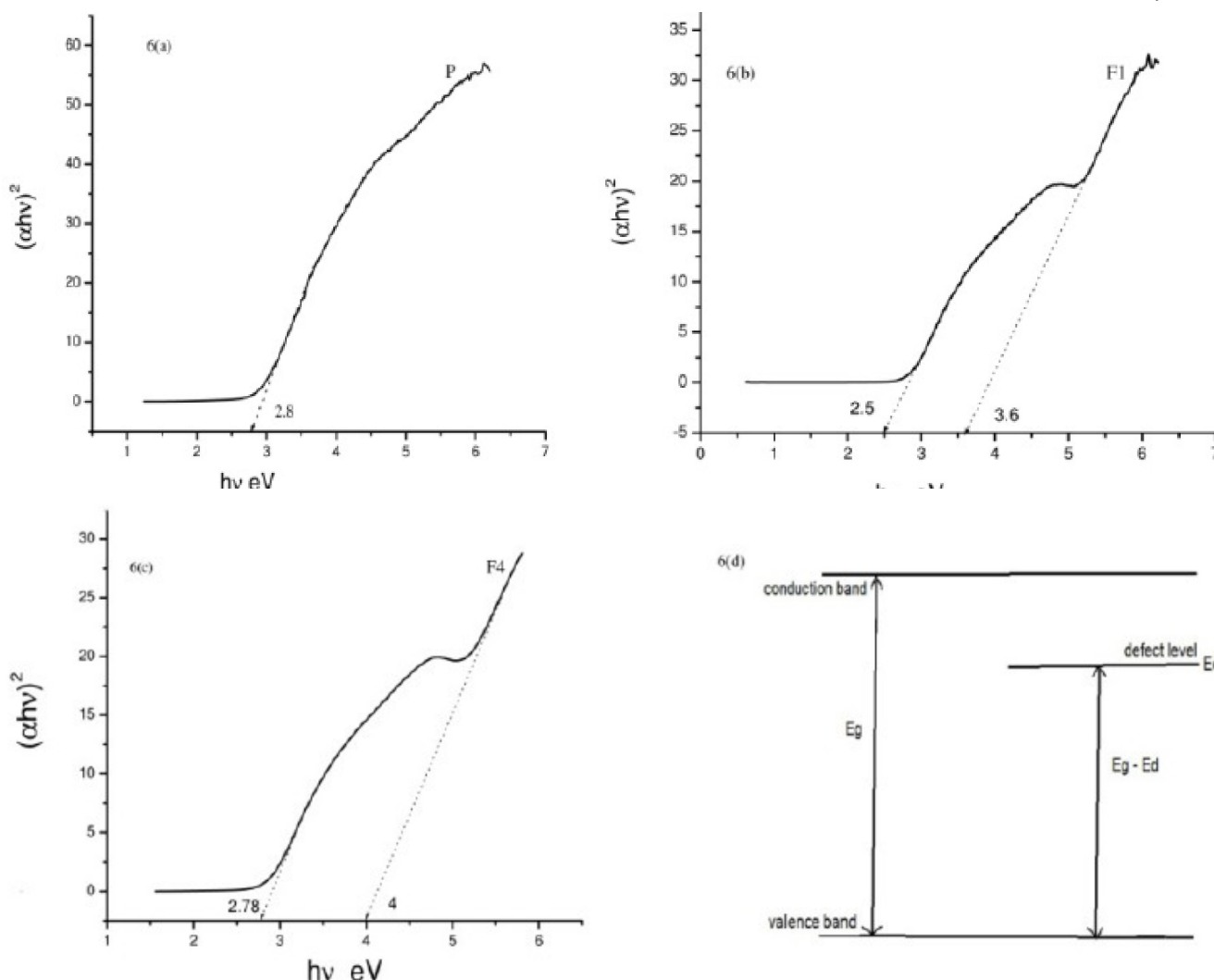
Figure 6 : Band gap for samples 6(a) P, 6(b) F1, 6(c) F4 and 6(d) schematic representation of defect levels created on doping. Band gap increases with doping
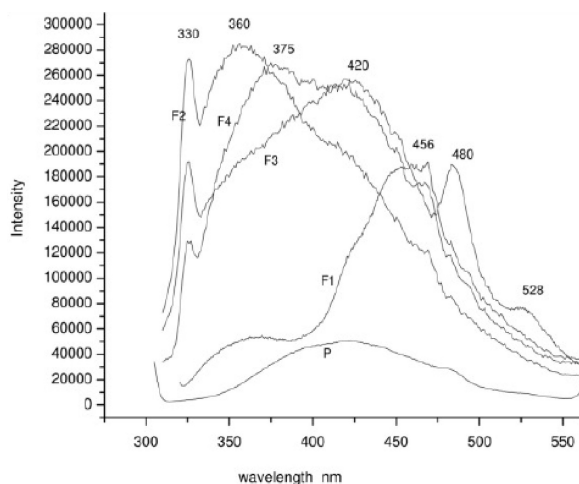

Figure 7 : PL spectra of samples P, F1, F2, F3 and F4. On doping more defect levels and oxygen vacancies are created, as a result emission intensity increases & extends from UV to visible

More clearly, energy levels formed by oxygen vacancies are above Ce '4f' band states and under Ce '5d' level. When the material is excited, valence band electrons make transition to the defect state within the band gap. From this defect state, the electron will undergo multiple transitions. Ce^{3+} ions present in the crystal lattice create a trap state above valence band and correspond to the Ce 5d-4f transition (blue emission) with high UV absorption due to allowed electric dipole transition and thus rare earth phosphate materials are good materials for photonic devices[15,19,22,23]. Peaks at 480 nm and 528 nm are characteristic peaks of Ce^{3+} state.

3.7 FT-IR studies

Fourier Transform Infrared (FT-IR) spectra of the samples in the transmittance mode were recorded in

Full Paper

the range of $400 - 4000$ cm^{-1} with a resolution of 4cm^{-1} on a Thermo Nicolet, Avatar 370 spectrophotometer, using KBr pellet method. The formation of desired crystal phases for different synthetic conditions can be observed from the infrared spectroscopic studies, Figure 8. In Cerium phosphate and other doped samples, a broad peak is observed at 3430 - 3130 cm^{-1} due to –OH stretch and peak at 1630 cm^{-1} is attributed to aquo (H –O-H) bending mode. Peak at 1400 cm^{-1} represents P – O stretch and δ POH, peak at 1060 cm^{-1} assignable to symmetrical stretching vibration due to $(PO_4)^{3-}$. Sharp peak at 625 cm^{-1} and 520 cm^{-1} can be due to metal oxide stretching vibration[1,4,5,14,24]. These bands are characteristic of hydrous Cerium phosphates [25,26]. No impurity phases could be observed in the spectrum, confirms purity of the prepared sample. Most of the peaks in the doped sample occur more or less in the same position except that observed at ≈ 3430 cm^{-1}. Samples F1 and F2 show this band at 3138 and 3160 cm^{-1}. This can be due to the non – stoichiometric oxygen content in cerium compounds and due to oxygen

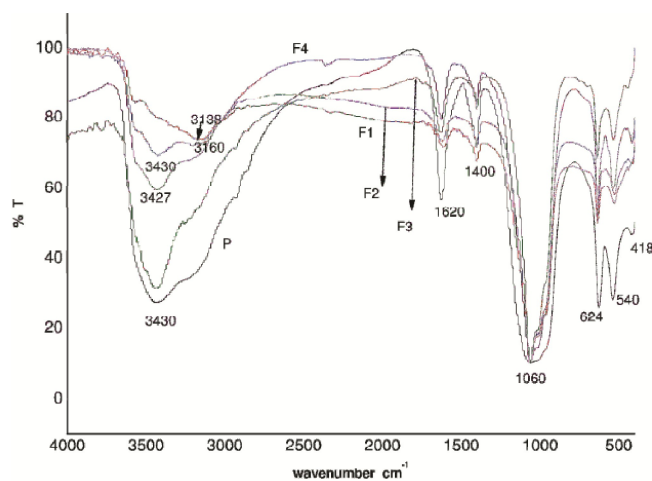Fig.8 FT-IR spectra of samples P, F1, F2, F3 and F4

exchange reactions[10,11]. EDS spectrum also shows a strong peak due to oxygen.

Raman studies

Raman scattering is a powerful characterizing technique used to analyze the lattice defect and the doping concentration of a material. Raman spectra were obtained using Raman spectrometers excited by an Ar$^+$ laser. The Raman spectra of undoped and doped samples are depicted in Figure 9.

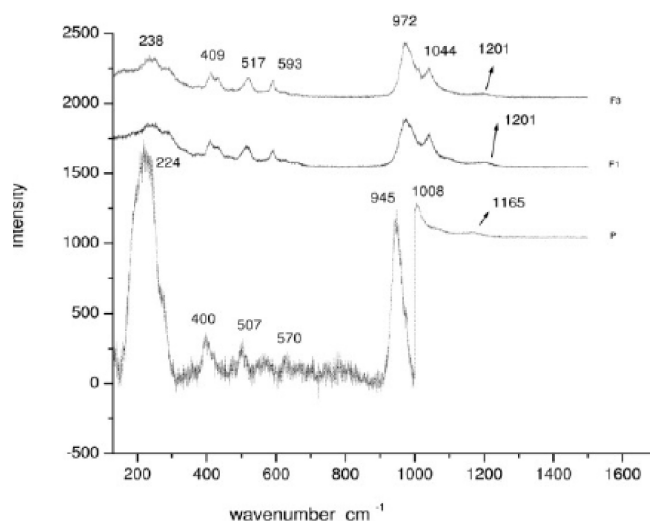Raman active bending vibrations υ_2 and υ_4 in the

Figure 9 : Raman spectra of samples P, F1 and F3

range $400 - 590$ cm^{-1}, were observed. This is the F_{2g} mode of cerium compounds[27]. Bands in the higher frequency range 945-1044 cm^{-1} corresponds to symmetric stretching vibrations υ_1 and υ_3 of phosphate group[28]. The lower frequency band 224 or 238 cm^{-1}, corresponds to the lattice mode of vibration which can be attributed to the vibrations of cations.

Ion exchange capacity (IEC) studies

The ion exchange capacity of the undoped sample was determined by column method[1,4,5,24]. The ion exchange capacity (IEC) of the exchanger, in milli equivalent per gram (meq gm^{-1}) is given by (av/w), where a is the molarity of NaOH solution, v the volume of NaOH required for titration and w the weight of the ion exchanger. Here, ion exchange capacity of cerium phosphate with alkali metal ions like Li$^+$, Na$^+$, K$^+$ and alkaline earth metal ions like Mg^{2+}, Ca^{2+}, Sr^{2+} and Ba^{2+} were studied and tabulated in TABLE 2. From the data obtained, it is clear that for univalent and divalent ions, the

TABLE 2 : Ion exchange capacity – univalent and divalent ions

Exchanged ion	Hydrated ionic radius (pm)	Exchange capacity (meq gm^{-1})
Li$^+$	340	0.28
Na$^+$	276	0.35
K$^+$	232	0.42
Mg^{2+}	700	0.34
Ca^{2+}	630	0.42
Sr^{2+}	610	0.50
Ba^{2+}	590	0.60

exchange capacity increases with decrease in hydrated ionic radii, which agrees well with values reported earlier [3,12,29,30].

Dielectric study

For dielectric studies, pellets were prepared using KBr Press M – 15. Dielectric studies were done with HIOKI – 3252 LCR meter. Dielectric property of nanomaterials is due to the different types polarizations present in the material and it is entirely different from that of bulk materials. In nanomaterials, both grain interior and grain boundary contribute to the total conductivity which affects the dielectric property[31]. AC electrical and dielectric properties of the prepared samples were analyzed by measuring capacitance (C), phase angle (Θ), the modulus of complex impedance (Z), dissipation factor (D) and quality factor (Q) of the samples using impedance spectroscopy over a frequency range 100 Hz to 1 MHz. For this, pellets of undoped and doped samples were prepared, using a combination of uniaxial and isostatic pressing. A 13mm diameter hardened steel pressing die was used and approximately 2 gm of the fine powdered sample was loaded into the die. It was pressed to 5 tons using a KBr Press model M – 15. No binder was used. The resulting pellets were used for the dielectric studies. Variation of dielectric constant, dielectric loss and conductivity with the signal frequency at room temperature for a frequency range 100 Hz to 1MHz is depicted in Figure 10 (a), (b), and (c). From Figure 10(a), it is clear that all the samples
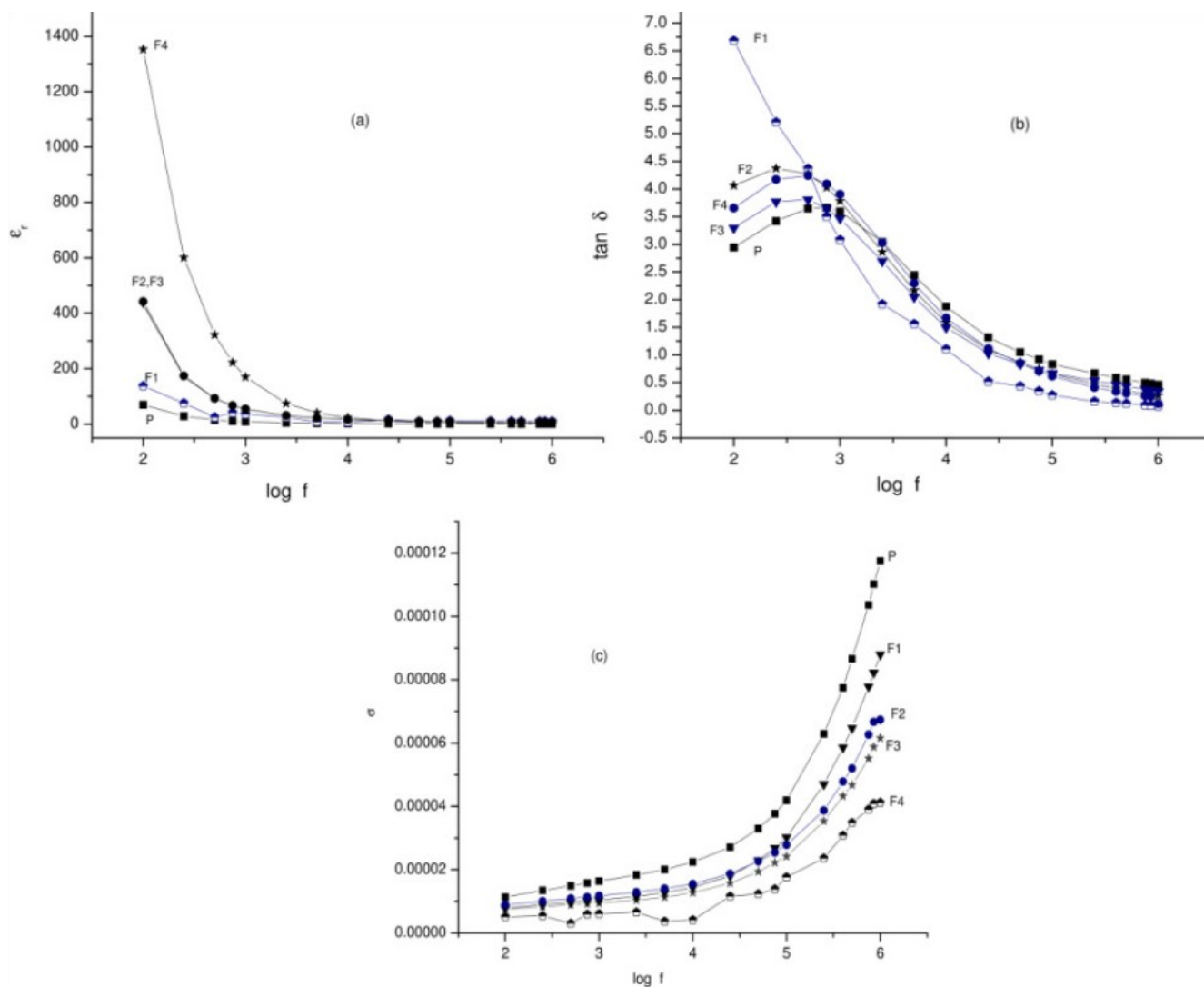

Figure 10 : Variation of (a) Dielectric constant (b) Loss tangent and (c) Conductivity with frequency. Dielectric constant increases with doping

Full Paper

exhibit high dielectric constant at low frequencies and decreases with the applied frequency. It is well known that nanocrystalline material consist of lot of grains or grain boundaries. Majority of the atoms reside in grain boundaries which contain defects such as dangling bonds, oxygen vacancies etc. These are responsible for space charge distribution at interfaces. On the application of external electric field, space charge can move and cause change of dipole moments, when they are trapped by the defects causes space charge polarization.

In addition to this, ions and vacancies play an important role in the dielectric behaviour of a material especially in cerium compounds owing to their redox properties ($Ce^{4+} \leftrightarrow Ce^{3+}$). When an electric field is applied, ions and oxygen vacancies can exchange positions which in turn produce change of dipole moments results in ion jump polarization. This leads to an increase in dielectric constant. Oxygen vacancies are very much equivalent to positive charges. When an electric field is applied, the dipoles get rotated, produces a resultant dipole moment in the direction of applied field produces rotation direction polarization. Rotation direction polarizations, ion jump polarization together with space charge polarization play a crucial role in deciding the dielectric property of a material[31] and they were responsible for high value of dielectric constant. Thus it can be concluded that high value of dielectric constant obtained in the present study can be due to the increased space charge polarization, rotation direction polarization and ion jump polarization. In our case, dielectric constant increases with doping. This may be due to the fact that doping increases the defects and oxygen vacancies which in turn increase polarization and thus dielectric constant. This was also evident from absorption spectra and photoluminescence spectra.

When an electric field is applied, space charge carriers in a dielectric material require enough time to line up their axes parallel to the applied electric field. At low frequencies dielectric will get sufficient time for this. As frequency increases beyond a particular value, the space charge carriers cannot keep in parallel with the field and they lag behind the field produces a decrease in polarization which results in low value of dielectric constant at high frequency and conductivity increases with frequency. These two are depicted in Figure 10(a) and 10(c).

The external field applied to the dielectric material is utilized

1   to overcome the internal frictional force and
2   for rotations of dipolar molecules and other kinds of molecular transfer from one position to another (ion jump), produces energy loss.

Dielectric loss occurs due to absorption of current. The defects, space charge formation and all the inhomogenities in nanomaterials cause absorption of current, which causes dielectric loss. The dangling bonds at the surface will be highly reactive and adsorb gases like oxygen and nitrogen which can cause dielectric loss. From Figure 10(b), it is clear that for sample F1 dielectric loss has high value at low frequencies and gradually decreases and beyond 250 kHz loss remains constant. For all other samples dielectric loss initially increases with frequency, attains a maximum value and then decreases at a slower rate.

CONCLUSION

Cerium phosphate, a luminescent cation exchanger in nano range is prepared by co – precipitation method. It was doped with zinc of different molarities. Samples were indexed and they belong to anorthic phase. No impurity phases could be observed from XRD, EDX, FT-IR studies. From the results of ion exchange study it is clear that Cerium phosphate seems to be a promising ion exchange material with a significant ion exchange capacity. The ion exchange capacity (IEC) in meq gm^{-1} for different metal ions are : Li^+, 0.28; Na^+, 0.35; K^+, 0.42; Mg^{2+}, 0.34; Ca^{2+}, 0.42; Sr^{2+}, 0.50; Ba^{2+}, 0.60. Diffuse reflectance study reveals that more defect levels were created and this was in close agreement with PL studies. From PL studies, it can be inferred that the emission spectra in the sample is due to the transition by

(i)   Ce 4f to O 2p level
(ii)   Defects level to O 2p and
(iii)   Ce 5d – 4f transition.

The prepared samples exhibit strong UV absorption with violet blue, green emission and therefore can be used as UV absorber, UV shielding materials, light emission diode, electroluminescence devices, non mercury fluorescent lamps. Raman active modes were observed in all samples. From dielectric study it is clear that doping increases dielectric constant and our sample

Full Paper

is a promising candidate for insulating material.

ACKNOWLEDGMENTS

REFERENCES

[1] A.Nilchi, B.Maleek, A.Khanchi., M.Ghanadi Maraghesh, A.Bagheri; Radiation Physics and Chemistry., **75**, 301 **(2006)**.

[2] Rakesh Thakkar, Heemanshu Patel, Uma Chudsama; Bull.Mater.Sci., **30**, 205 **(2007)**.

[3] Weqar Ahmad Siddiqui, Shakeel Ahmad Khan; Bull.Mater.Sci., **30**, 43 **(2007)**.

[4] Beena Pandit, Uma Chudasama; Bull.Mater.Sci., **24**, 265 **(2001)**.

[5] Amin Jignasa, Thakkar Rakesh, Chudasama Uma; J.Chem.Sci., **118**, 185 **(2006)**.

[6] Rakesh Thakkar, Uma Chudsama; Journal of Scientific & Industrial Research., **68**, 312 **(2009)**.

[7] C.R.Indulal, G.Sajeev Kumar, A.V.Vaidyan, R.Raveendran; Indian Journal of Pure and Applied Physics., **48**, 893 **(2010)**.

[8] C.R.Indulal, R.Raveendran; Indian Journal of Pure and Applied Physics., **48**, 121 **(2010)**.

[9] C.R.indulal, A.V.Vaidyan, G.Sajeev Kumar, R.Raveendran; Indian Journal of Engineering and Material Sciences., **17**, 299 **(2010)**.

[10] Uy.D.A.E.O' Neill, L.Xu, W.H.Weber, R.W.McCabe; Applied Catalysis B: Environmental., **41**, 269 **(2003)**.

[11] Ling Meng, Lige Yang, Bo Zhou, Chenxin Cai; Nanotechnology., **20**, 1 **(2009)**.

[12] G.Kottim; Reflectance Spectroscopy, Springer Verla, New York, **(1969)**.

[13] W.Wendlandt, H.Hecht; Reflectance Spectroscopy, Wiley Interscience, New York, **(1966)**.

[14] Yan Xing, Mei Li, Sean A.Davis, Stephen Mann; J.Phys.Chem.B., **110**, 1111 **(2006)**.

[15] Chengchun Tang, Yoshio Bando, Dimitri Golberg, Renzhi Ma; Angrew.Chem.Int.Ed., **44**, 576 **(2005)**.

[16] Takeshi Morimoto, Hiroyuki Tomonaga, Akemi Mitani; Thin Solid Films., **351**, 61 **(1999)**.

[17] Srivatsan Sathyamurthy, Keith J.Leonard, Reza T.Dabestani, M.Parans Paranthaman; Nanotechnology., **16**, 1960 **(2005)**.

[18] A.Alifatima, Suganthi Devadason; J.Pure Appl.& Ind.Phys., **1**, 115 **(2011)**.

[19] Chai Chunlin, Yang Shaoyan, Liuzhikai, Liao Meiyng, Chen Nuofu; Chinese Sci.Bull., **48**, 1198 **(2003)**.

[20] Mingyun Guan, Jianhua Sun Tongming Shang, Quanfa Zhou, Jianting Han, Aiqin Ji; J.Mater.Sci.Technol., **26**, 45 **(2010)**.

[21] Satya Prakash; Advanced Chemistry of Rare Elements, S.Chand & Company Ltd, New Delhi, **(1986)**.

[22] R.Martinez–Martinez, M.Garcia–Hipolito, F.Ramos–Brito, J.L.Hernandez–Pozos, U.Caldino Falcony; J.Physics: Condense.Mater., **17**, 3647 **(2005)**.

[23] Amita Verma, Amish G.Joshi; Indian J.Chem., **48A**, 161 **(2009)**.

[24] Heemanshu Patel, Uma Chudasama; J.Chem.Sci., **119**, 35 **(2007)**.

[25] Kauzuo Nakamoto; Infrared and Raman Spectra of Inorganic and co–ordination compounds, Fourth Edn, A Wiley-Interscience Publication, **(1986)**.

[26] Adly Abdella Hanna, Sahar Mohamed Mousa, Gehan Mahmoud Elkomy, Marwa Abdul Sherief; Eur.J.Chem., **1**, 211 **(2010)**.

[27] W.H.Weber, K.C.Hass, J.R.McBride; Physical Review B., **48**, 178 **(1993)**.

[28] Adrian Borhan, Bogdan Apetrachioaei, Karin Popa; Rev.Roum.Chim., **55**, 389 **(2010)**.

[29] S.A.Nabi, R.K.Rao; J.Indian Chem.Soc., **58**, 1030 **(1981)**.

[30] Premvir Singh, J.P.Rawat, N.Rahman; Talanta., **59**, 443 **(2003)**.

[31] B Tareev; Physics of Dielectric Materials, Mir Publishers, Moscow, **(1979)**.